

Maximum-Likelihood Circle-Parameter Estimation via Convolution

Emanuel E. Zelniker* and I. Vaughan L. Clarkson

Intelligent Real-Time Imaging and Sensing Group
School of Information Technology and Electrical Engineering
University of Queensland, QLD 4072, AUSTRALIA.
(zelniker,v.clarkson)@itee.uq.edu.au

Abstract In this paper, we present an interpretation of the Maximum Likelihood Estimator (MLE) and the DELOGNE-KÁSA Estimator (DKE) for circle-parameter estimation via convolution. Under a certain model for theoretical images, this convolution is an exact description of the MLE. We use our convolution based MLE approach to find good starting estimates for the parameters of a circle, that is, the centre and radius. It is then possible to treat these estimates as preliminary estimates into the NEWTON-RAPHSON method which further refines these circle estimates and enables sub-pixel accuracy. We present closed form solutions to the CRAMÉR-RAO Lower Bound of each estimator and discuss fitting circles to noisy points along a full circle as well as along arcs. We compare our method to the DKE which uses a least squares approach to solve for the circle parameters.

1 Introduction

The estimation of the centre and radius of a circle given noisy circular data points which lie on its circumference is a very well known problem. It often arises in digital image processing when circular features in digital images are sought. The reasons for this range from quality inspection for mechanical parts [1] to fitting circles for particle trajectories [2].

One of the early applications of circle fitting was studied by ROBINSON [3] in connection to fitting circles to a set of noisy coplanar points. His method is based on a least squares approach. Circle fitting also has applications in archaeology [4], microwave engineering [5] and ball detection in robotic vision systems [6].

An advantage of working with images rather than with data points directly is that it is a lot more convenient. Often it is desirable to perform the circle parameter estimation on images directly rather than somehow extracting the x and y coordinates of each noisy circle point in the image and performing Maximum Likelihood Estimation (MLE) or a least squares fit on the points themselves. It would be very useful to express the MLE and the least squares procedure in terms of convolution.

* Emanuel Zelniker is additionally supported by a scholarship from the Commonwealth Scientific & Industrial Research Organisation.

KERBYSON & ATHERTON [7] mention that the Hough transform can be implemented by convolving a single circle with an edge magnitude image. They build on this idea by defining an orientation annulus which detects a range of radii of circles, but also uses edge orientation information by taking the dot-product between the edge orientation and an orientation field within the annulus. A phase coded annulus is also described which detects a range of radii of circles by using phase to code for radius. Combining this with the orientation annulus operator results in a circle detection operation which uses both edge orientation information and size information. The operator is applied by using convolution.

In this paper, we present an interpretation of the MLE and the Delogne-Kåsa Estimator (DKE) which uses linear least squares [8] via convolution. In an ideal image, which we define as an unbounded image with continuous-values in intensity and in spatial coordinates, we show that the minimum of the convolution gives the precise MLE for circle centre. In a digital image, the convolution gives a necessarily coarser estimate. However, this can be used as a starting point for the NEWTON-RAPHSON method in order to obtain sub-pixel accuracy.

We give a brief outline of CHAN's circular functional model in (§2) and in (§3), we give a brief outline of the MLE. We then show the connection between the classical formulation of the MLE and DKE and the new interpretation in terms of convolution (§4). We present closed form solutions to the CRAMÉR-RAO Lower Bound of each estimator and discuss fitting circles to noisy points along a full circle as well as along arcs in (§5). We compare our method to the DKE circle fitting procedure in (§6).

2 Chan's Circular Functional Model

In this Section, we briefly present CHAN's circular functional model [9]. In this model, we assume that the positions of N points on the circumference of a circle are measured. The measurement process introduces random errors so that the Cartesian coordinates (x_i, y_i) , $i = 1, \dots, N$ can be expressed as

$$x_i = a + r \cos \theta_i + \xi_i, \quad y_i = b + r \sin \theta_i + \eta_i.$$

Here, (a, b) is the centre of the circle, r is its radius, the θ_i are the angles around the circumference on which the points lie and the ξ_i and η_i are instances of random variables representing the measurement error. They are assumed to be zero-mean and i.i.d. In addition, we will specify that they are Gaussian with variance σ^2 .

Figure 1 shows some data with N points (or candidates) for the circumference of a circle and an arc, p_1, \dots, p_N , displaced from the circumference by noise. We explicitly exclude the possibility that $r = 0$ or $\theta_1 = \theta_2 = \dots = \theta_N$.

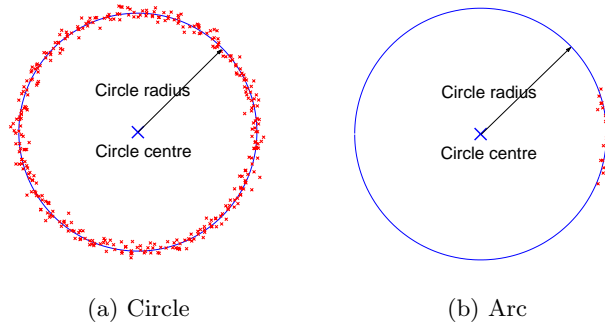


Figure 1. Noisy measurements of points on the circumference of a circle and an arc.

3 Maximum Likelihood Estimation (MLE)

The conditional probability density function for p_1, \dots, p_N in polar coordinates is as follows

$$P(p_1, \dots, p_N | a, b, r, \theta_1, \dots, \theta_N) = \frac{1}{(2\pi\sigma^2)^N} \prod_{i=1}^N \exp\left(-\frac{[x_i - (a + r \cos \theta_i)]^2 + [y_i - (b + r \sin \theta_i)]^2}{2\sigma^2}\right). \quad (1)$$

By definition, maximum likelihood estimates are given by those $\hat{a}, \hat{b}, \hat{r}, \hat{\theta}_1, \dots, \hat{\theta}_N$ that minimise (1).

We can consider the logarithm of (1) and obtain an objective function which is related to the log-likelihood by a scaling factor and constant offset, both of which depend only on σ and N . The objective function of the log-likelihood is the following sum which is a function of polynomials in a and b

$$f_{\text{obj}}(a, b, r, \theta_1, \dots, \theta_N | p_1, \dots, p_N) = -\sum_{i=1}^N [x_i - (a + r \cos \theta_i)]^2 + [y_i - (b + r \sin \theta_i)]^2. \quad (2)$$

Differentiating (2) with respect to θ_i and equating to zero, we find that the sum is minimised when

$$\theta_i = \arctan\left(\frac{y_i - b}{x_i - a}\right). \quad (3)$$

Substituting (3) into (2) and partially differentiating with respect to r shows that the radius estimate is the average of the distances from each noisy point to the centre, or

$$\hat{r} = \frac{1}{N} \sum_{i=1}^N \|p_i - c\|_2. \quad (4)$$

Hence, using (4), it is possible to express (2) as follows

$$f_{\text{obj}}(a, b | p_1, \dots, p_N) = - \sum_{i=1}^N \|p_i - c\|_2^2 + \frac{1}{N} \left[\sum_{i=1}^N \|p_i - c\|_2 \right]^2. \quad (5)$$

4 MLE via Convolution

4.1 Ideal Images

We define an ideal image of our noisy circular points as one which is unbounded and which is continuous-valued in intensity and in spatial coordinates. Under these conditions, we can assume that the points are represented by 2-dimensional delta functions, that is, we can consider the image as a function $f(x, y)$, where

$$f(x, y) = \sum_{i=1}^N \delta(x - x_i, y - y_i). \quad (6)$$

If we define a 2-dimensional kernel function (represented graphically in Figure 2(a)) as $g(x, y) = \sqrt{x^2 + y^2}$ then $f(x, y) * g^0(x, y) = N$ and

$$f(x, y) * g(x, y) = \sum_{i=1}^N g(x - x_i, y - y_i) = \sum_{i=1}^N \|p_i - c\|_2, \quad (7)$$

$$f(x, y) * g^2(x, y) = \sum_{i=1}^N g^2(x - x_i, y - y_i) = \sum_{i=1}^N \|p_i - c\|_2^2. \quad (8)$$

It then follows that

$$f_{\text{obj}}(a, b | p_1, \dots, p_N) = f(a, b) * g^2(a, b) - \frac{(f(a, b) * g(a, b))^2}{f(a, b) * g^0(a, b)}. \quad (9)$$

That is, (9) is an exact interpretation of equation (5). The MLE is therefore shown to be equivalent to minimising the intensity of an ideal image obtained through convolution. It is known that the MLE is the best estimator for circle parameters in a certain range of signal to noise ratio.

4.2 Real Images

For real digital images, the assumptions in Section 4.1 do not hold. Digital images have a finite resolution and can only be of a certain size. As a result, our model is not entirely accurate, but it can still be applied to real images. If we have a digital image $f[x, y]$ and a conic kernel $g[x, y]$ (where the square brackets $[\cdot]$ denote the discretised version of the image in (6) and the kernels in Figure 2) then we can still implement the following equation

$$f_{\text{obj}}(a, b | p_1, \dots, p_N) = f[a, b] * g^2[a, b] - \frac{(f[a, b] * g[a, b])^2}{f[a, b] * g^0[a, b]}. \quad (10)$$

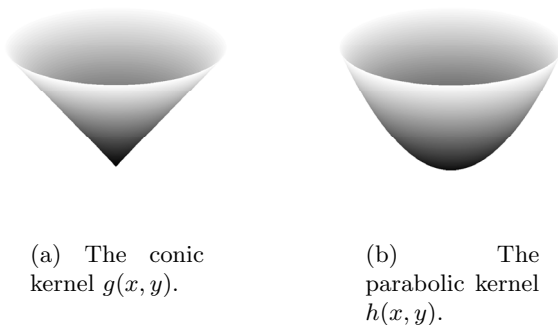


Figure 2. Convolution kernels in MLE and LLS.

Equation (10) on its own is suitable to provide a coarse estimate of the circle-centre. However, if sub-pixel accuracy is required in the parameter estimates, we propose that equation (10) can be used as a mechanism by which to start the NEWTON-RAPHSON method. Equation (10) will return a 2-dimensional intensity image, the minimum of which will be the coarse centre estimate. This can then be treated as a starting point for the NEWTON-RAPHSON method. On its own, the NEWTON-RAPHSON method is very well known to get stuck in local minima because the starting point is chosen incorrectly (usually it will be chosen in an ad-hoc manner by the user) or it can diverge to $\pm\infty$ or even oscillate between two points without converging at all. By implementing (10) first, we can be more confident that the NEWTON-RAPHSON method will reach the global minimum. We can then use equation (4) to obtain the radius estimate, \hat{r} .

The advantages of running our algorithm on real digital images are that in many situations, the size of the circle one is trying to detect is known and therefore, the user can impose a constraint on the maximum size (radius) of the circle. Moreover, circles of any size up to the maximum radius constraint can be detected in images provided they do not overlap.

4.3 DKE via Convolution

It is also possible to express the DKE [8] as a convolution equation under the assumptions in Section 4.1. The paper in [8] shows that the DKE is a biased estimator however, as $\sigma \rightarrow 0$, the DKE is shown to be unbiased and statistically efficient. This estimator was used by KÅSA [5] and originally proposed by DELOGNE [10] and can be written as follows

$$(\hat{a}_{DK}, \hat{b}_{DK}, \hat{r}_{DK}) = \arg \min_{(a,b,r)} \sum_{i=1}^N [(x_i - a)^2 + (y_i - b)^2 - r^2]^2. \quad (11)$$

A partial derivative shows that the sum is minimised when

$$\hat{r}_{DK}^2 = \frac{1}{N} \sum_{i=1}^N (x_i - a)^2 + (y_i - b)^2. \quad (12)$$

Substituting (12) into (11) and simplifying results in the following expression

$$(\hat{a}_{DK}, \hat{b}_{DK}) = f(x, y) * h^2(x, y) - \frac{(f(x, y) * h(x, y))^2}{f(x, y) * h^0(x, y)}, \quad (13)$$

where $h(x, y) = g^2(x, y)$. This can be interpreted as a 2-dimensional intensity image, the minimum of which is the centre estimate.

In order to implement (13) on a digital image, we would need to replace $f(x, y)$ and $h(x, y)$ with $f[a, b]$ and $h[a, b]$ respectively.

5 Cramér-Rao Lower Bound (CRLB)

In order to statistically analyse the convolution based MLE, we make use of the the CRAMÉR-RAO Lower Bound (CRLB). This provides a theoretical lower bound for the variance of each estimator for a certain amount of noise, σ , present in the circular data points.

From VAN TREES [11], it can be shown that by calculating the FISHER INFORMATION MATRIX, \mathbf{J} , the entries along the main diagonal of \mathbf{J}^{-1} will correspond to the lower bound of the variance of each estimator, $\sigma_{\hat{a}}^2, \sigma_{\hat{b}}^2, \sigma_{\hat{r}}^2, \sigma_{\theta_1}^2, \dots, \sigma_{\theta_N}^2$. Since we are only interested in the CRLB of \hat{a} , \hat{b} and \hat{r} , it is of interest to obtain the upper 3×3 sub-matrix of \mathbf{J}^{-1} . If we denote \mathbf{J}_{11} as the upper 3×3 sub-matrix of \mathbf{J} , then \mathbf{J}_{12} , \mathbf{J}_{21} and \mathbf{J}_{22} are $3 \times N$, $N \times 3$ and $N \times N$ respectively and are the remaining sub-matrices of \mathbf{J} . CHAN & THOMAS [12] showed that

$$\mathbf{J}_{11} - \mathbf{J}_{12}\mathbf{J}_{22}^{-1}\mathbf{J}_{21} = \frac{1}{\sigma^2} \sum_{i=1}^N \begin{pmatrix} \cos^2 \theta_i & \cos \theta_i \sin \theta_i & \cos \theta_i \\ \cos \theta_i \sin \theta_i & \sin^2 \theta_i & \sin \theta_i \\ \cos \theta_i & \sin \theta_i & 1 \end{pmatrix}, \quad (14)$$

but see also [13] for a more straight forward derivation. If we assume that the θ_i are equally spaced around the circle and define θ_i as follows

$$\theta_{i+1} = \frac{i\phi}{N} + \frac{\phi}{2N} - \frac{\phi}{2}, \quad i = 1, \dots, N - 1, \quad (15)$$

where ϕ can be anything from 0 to 2π radians, we can investigate the CRLB of our estimates for full circles as well as arcs. The closed form solutions to the entries in (14) will be

$$\mathbf{J}_{11} - \mathbf{J}_{12}\mathbf{J}_{22}^{-1}\mathbf{J}_{21} = \frac{1}{\sigma^2} \begin{pmatrix} \frac{N}{2} + \frac{\sin \phi}{2 \sin \frac{\phi}{N}} & 0 & \frac{\sin \frac{\phi}{2}}{\sin \frac{\phi}{2N}} \\ 0 & \frac{N}{2} - \frac{\sin \phi}{2 \sin \frac{\phi}{N}} & 0 \\ \frac{\sin \frac{\phi}{2}}{\sin \frac{\phi}{2N}} & 0 & N \end{pmatrix}, \quad (16)$$

and therefore

$$(\mathbf{J}_{11} - \mathbf{J}_{12}\mathbf{J}_{22}^{-1}\mathbf{J}_{21})^{-1} = \sigma^2 \begin{pmatrix} \frac{2}{N-\psi} & 0 & f(\phi, N) \\ 0 & \frac{2}{N-\xi} & 0 \\ f(\phi, N) & 0 & \frac{1}{N-\Omega} \end{pmatrix}, \quad (17)$$

where $f(\phi, N)$ is a function in terms of ϕ and N and

$$\Psi = \frac{2 \sin^2 \frac{\phi}{2}}{N \sin^2 \frac{\phi}{2N}} - \frac{\sin \phi}{\sin \frac{\phi}{N}}, \quad \Xi = \frac{\sin \phi}{\sin \frac{\phi}{N}}, \quad \Omega = \frac{2 \sin^2 \frac{\phi}{2} \sin \frac{\phi}{N}}{\sin^2 \frac{\phi}{2N} (N \sin \frac{\phi}{N} + \sin \phi)}. \quad (18)$$

The lower bounds of the variance of \hat{a} , \hat{b} and \hat{r} lie along the main diagonal of (17).

Having a closer look at equation (17), it can be seen that if ϕ is equal to 2π radians, then the CRLB for \hat{a} , \hat{b} and \hat{r} vary linearly with σ . However, if ϕ describes an arc than there will be what we refer to as correction factors in the denominator along the main diagonal, Ψ , Ξ and Ω respectively. If we plot Ψ , Ξ and Ω from 0 to 360° , we obtain the plots in Figure 3. From these plots, it can be seen that when ϕ is less than 2π radians, the CRLB for each estimator increases. This also makes sense intuitively because as the arc length decreases, it becomes more difficult to fit a circle to the noisy data points along the arc.

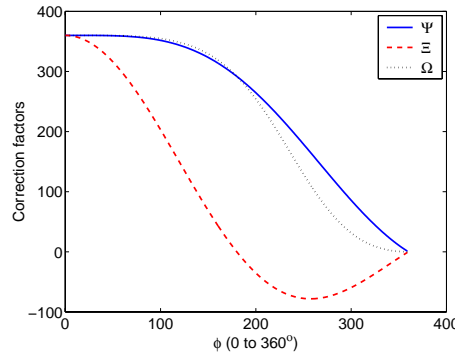


Figure 3. A plot of the correction factors as a function of ϕ for $N = 360$ points. If N changes, the y-axis of the plot will be scaled accordingly.

A very interesting observation can be made about the CRLB of the estimator \hat{b} . When ϕ is between π and 2π radians, the CRLB for σ_b^2 can actually be lower than $2\sigma^2/N$ which is the CRLB for \hat{b} when ϕ equals 2π radians, something that is not so intuitive. This behaviour can be explained by looking at concentration ellipses. From VAN TREES [11], concentration ellipses are regions inside which the probability, P of the error vector is a certain amount, say, the 99% confidence ellipse. It is possible to plot these concentration ellipses for different values of ϕ in the case of the 99% confidence level, *i.e.* $P = 0.99$. The major and minor axes will be the CRLB for \hat{a} and \hat{b} respectively. Setting N to 360, σ to 5 and ranging ϕ from $\pi/4$ to 2π radians, the ellipses are plotted in Figure 4. It can be clearly seen that for the ellipses corresponding to ϕ between π and 2π radians, the CRLB of \hat{b} is less than the CRLB of \hat{b} when $\phi = 2\pi$ radians. This explains the behaviour of the plot for Ξ in Figure 3 for ϕ between π to 2π radians.

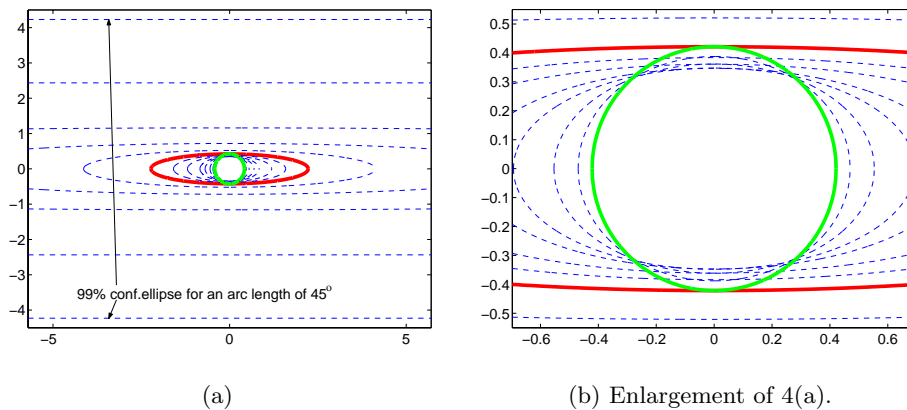


Figure 4. 99% confidence ellipses for various values of arc length ϕ . The bold and solid lined ellipse and circle correspond to the confidence ellipses for an arc length of π and 2π radians respectively.

6 Simulations and Results

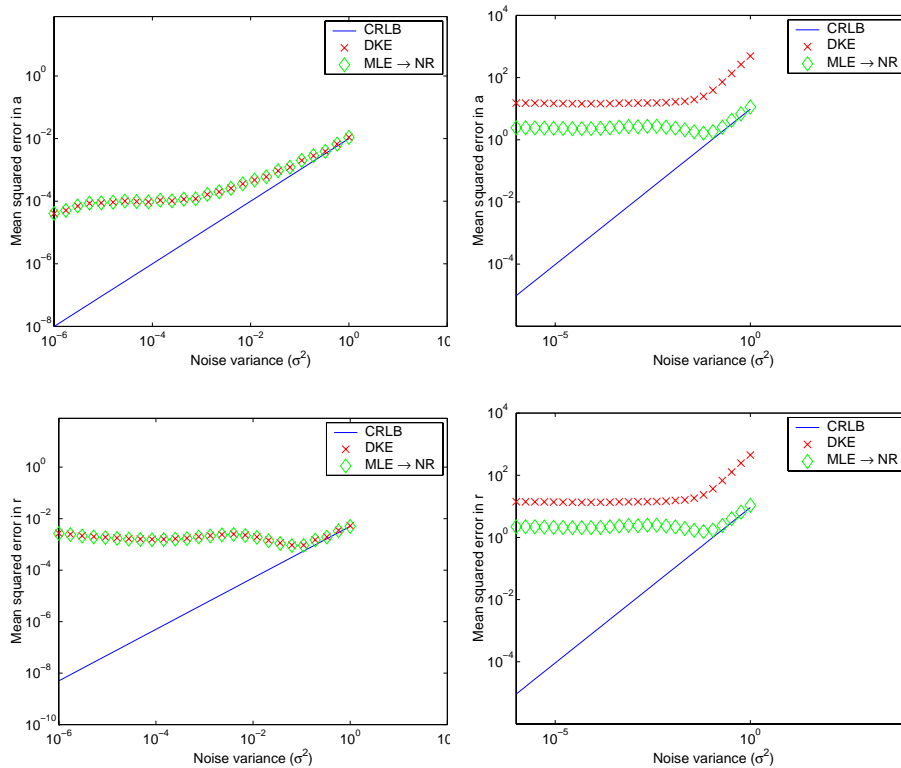
This section will present a MONTE-CARLO analysis to compare the DKE circle fitting procedure [8] to our method as a starting point for the NEWTON-RAPHSON method.

For the DKE, in each trial, 200 points ($N = 200$) were generated in equal increments around a full circle as well as an arc length, ϕ of $\pi/4$ radians. The radius r was set to 50. Then, noise was added to each (x_i, y_i) coordinate pair in the form of (ξ_i, η_i) . The amount of noise, σ was varied from 10^{-3} to 1 in equal geometric increments. Quantisation noise was added on top of this so that we could compare the DKE to the MLE in a fair way. Then, the DKE was run repeatedly, 750 times, for each value of σ to obtain estimates for the centre of the circle (\hat{a}, \hat{b}) and \hat{r} and use them to generate mean square error values. These values were then plotted against their corresponding theoretical CRLB for the same level of noise σ . The plots can be seen in Figure 5 on a logarithmic scale (crosses). The plot for \hat{b} follows a similar pattern to that for \hat{a} and is omitted for this reason.

In addition to this and on the same plots, for each value of ϕ and σ , MONTE-CARLO simulations were performed for our convolution equation (10) as a starting point to the NEWTON-RAPHSON method. Again, N was set to 200 points and noise was added in the same way. Because this method involved convolution with discrete images, each point needed to be rounded off to the nearest grid position in the digital image, which was chosen to be 121×121 in size. In other words, in addition to the white Gaussian noise added to each point, quantisation noise was also added. If, after the addition of quantisation noise, certain points became stacked on top of each other, the intensity value at the corresponding grid position in the image was incremented by the necessary amount. Our al-

gorithm was run repeatedly, 750 times for each value of σ , to obtain estimates for (\hat{a}, \hat{b}) and \hat{r} . Mean square error values were generated and the results are plotted in Figure 5 (in diamonds) against the corresponding theoretical CRLB for the same level of noise σ . Again, the plot for \hat{b} follows a similar pattern to that for \hat{a} and is therefore omitted. When an image was convolved with a certain kernel, the multiplication of their respective spectrums was performed, followed by an inverse FFT. FFT algorithms for images with N rows are known to be $N^2 \log_2(N)$ in complexity.

The effect of quantisation noise is that at a certain value for σ , the simulation results level off and stop adhering to the CRLB. It can be seen that as ϕ decreases and the amount of noise σ increases, the MLE NEWTON-RAPHSON method adheres to the theoretical CRLB more closely than the DKE method.



(a) Results for $\phi = 360^\circ$.

(b) Results for $\phi = 45^\circ$.

Figure 5. MONTE-CARLO simulation results.

7 Conclusion

We have presented a new interpretation of the MLE and DKE for circle parameter estimation which uses a convolution based approach to solve for the centre estimate. For the MLE, the output provides a coarse estimate, but in order to obtain sub-pixel accuracy, it is possible to refine the coarse estimate through the NEWTON-RAPHSON method to achieve sub-pixel accuracy. A comparison of the MLE NEWTON-RAPHSON method to the DKE least squares method shows that the MLE performs better as the arc length gets smaller and as the noise level gets larger. We would like to point out that our motivation in writing this paper was to investigate accurate and optimal circle fitting methods and not ones which are fast. We would also like to point out that our algorithm is not designed for overlapping circles in images or for ‘natural’ scenes which contain edge points of non-circular objects. The problem of grouping circular edge detected points in images and ignoring edge points which are not part of the circle is still an open problem and is yet to be fully investigated. This is something that the authors intend to pursue.

References

1. Landau, U.M.: Estimation of a Circular Arc Center and its Radius. *Comput. Vision Graph. Image Process.* **38** (1986) 317–326
2. Karimäki, V.: Effective circle fitting for particle trajectories. In: *Nucl. Instru. Methods Phys. Research.* (1991) 187–191
3. Robinson, S.M.: Fitting Spheres by the Method of Least Squares. In: *Comm. ACM.* (1961) 491
4. Thom, A.: A Statistical Examination of the Megalithic Sites in Britain. *J. Roy. Statist. Soc. Ser. A General* **118** (1955) 275–295
5. Kåsa, I.: A circle fitting procedure and its error analysis. **25** (1976) 8–14
6. Coath, G., Musumeci, P.: Adaptive Arc Fitting for Ball Detection in Robocup, Brisbane, Australia (2003) 63–68
7. Kerbyson, D.J., Atherton, T.J.: Circle Detection Using Hough Transform Filters. In: *Image Process. Appl.* (1995) 370–374
8. Zelniker, E.E., Clarkson, I.V.L.: A Statistical Analysis of the DELOGNE-KÅSA Method for Fitting Circles. Submitted to *IEEE Trans. Signal Process.* (2003)
9. Chan, N.N.: On Circular Functional Relationships. *J. Roy. Statist. Soc. Ser. B Stat. Methodol.* **27** (1965) 45–56
10. Delogne, P.: Computer Optimization of Deschamps’ method and error cancellation in reflectometry. In: *Proc. IMEKO-Symp. Microwave Measurements, Budapest, Hungary* (1972) 117–123
11. Van Trees, H.L.: *Detection, Estimation and Modulation Theory, Part 1.* Wiley, New York (1968)
12. Chan, Y.T., Thomas, S.M.: Cramér-Rao Lower Bound for Estimation of a Circular Arc Center and its Radius. (1995) 527–532
13. Kanatani, K.: Cramér-Rao Lower Bounds for Curve Fitting. In: *Graph. Models Image Process.* (1998) 93–99